

ANALYSIS OF A HYBRID CURRENT MODULATED DUAL ACTIVE BRIDGE PHOTOVOLTAIC DC/DC CONVERTER FOR UNIFORM IRRADIATION CONDITIONS

Sinan ZENGİN*, Electrical and Electronics Engineering Department, Ege University, Turkey,
sinan.zengin@ege.edu.tr

( <https://orcid.org/0000-0002-7357-4836>)

Received: 28.08.2023, Accepted: 17.05.2024

Research

*Corresponding author

DOI: 10.22531/muglajsci.1351487

Abstract

The energy of Photovoltaic (PV) modules can be connected to DC grid with high step-up ratio power electronics converters. Generally, two-stage isolated boost-based converters are used for this purpose. However, these types of converters consist of a high number of semiconductors which must withstand high voltage levels, and they utilize input inductance which has high value and large magnetic core size. To solve these problems, single-stage conversion-based Hybrid Current Modulated (HCM) isolated Dual Active Bridge (DAB) converter is proposed in the literature. However, this converter is designed for considering partial shading (PS), and PS rarely occurs in PV farms. In this study, the design methodology of DAB PV DC/DC converter is given for uniform irradiation (UI) conditions that is more suitable for PV farms. In addition, UI and PS designs of HCM DAB PV DC/DC converter are compared to each other. Analyses show that UI-based design has 3.88% smaller RMS² current, 3.56% smaller peak current and 2.35% smaller core size than the PS-based design. Hence, UI-based design can be more efficient, cheaper, and smaller in size.

Keywords: DAB converter, Hybrid current modulation (HCM), Photovoltaic (PV) energy conversion, Uniform Irradiation (UI) conditions

ÜNİFORM IŞINIM KOŞULLARI İÇİN BİR HİBRİT AKIM MODÜLASYONLU ÇİFT AKTİF KÖPRÜ FOTOVOLTAİK DC/DC DÖNÜŞTÜRÜCÜNÜN ANALİZİ

Özet

Fotovoltaik (PV) modüllerin enerjisi yüksek dönüşüm oranlı güç elektroniği dönüştürücüleri ile DC şebekeye bağlanabilir. Genellikle bu amaç için iki-aşamalı izoleli boost-tabanlı dönüştürücüler kullanılmaktadır. Fakat bu tipteki dönüştürücüler, yüksek gerilim seviyelerine dayanması gereken yüksek sayıda yarı-iletken anahtar içermekte ve yüksek endüktans değerine sahip büyük manyetik nüve boyutlu giriş bobini kullanmaktadır. Bu problemleri çözmek için, tek-aşamalı hibrit akım modülasyonlu çift aktif köprü (DAB) izoleli dönüştürücü literatürde önerilmiştir. Fakat bu dönüştürücü kısmi gölgeleme (PS) dikkate alınarak tasarlanmıştır ve PS PV tarlalarında nadiren oluşmaktadır. Bu çalışmada, DAB PV DC/DC dönüştürücün PV tarla çalışmalarında daha uygun olan üniform ışınım (UI) koşulları için tasarım metodolojisi verilmiştir. Ek olarak, HCM DAB PV DC/DC dönüştürücünün UI ve PS'ye ait tasarımları birbiri ile karşılaştırılmıştır. Analizler göstermektedir ki UI-tabanlı tasarım PS-tabanlı tasarıma göre %3.88 daha küçük RMS² akım, %3.56 daha küçük tepe akımı, %2.35 daha küçük nüve boyutuna sahiptir. Dolayısı ile UI-tabanlı tasarım daha verimli, daha ucuz ve boyut açısından daha küçük olabilir.

Anahtar Kelimeler: Çift aktif köprü (DAB) dönüştürücü, hibrit akım modülasyonu (HCM), Fotovoltaik (PV) enerji dönüşümü, Üniform ışınım koşulları

Cite

Zengin, S., (2024). "Analysis of a Hybrid Current Modulated Dual Active Bridge Photovoltaic DC/DC Converter for Uniform Irradiation Conditions", *Mugla Journal of Science and Technology*, 10(1), 82-88.

1. Introduction

Due to modularity of Photovoltaic (PV) modules, it can be used in small power roof-top or utility scale systems. Therefore, the installed PV energy capacity in 2027 is expected to be the largest renewable energy system among other renewables [1].

PV systems can be connected to the grid or operate stand-alone. Stand-alone systems require heavy and expensive battery systems, so 99% of PV systems are installed as AC or DC grid-connected [2]. Since PV output is DC, DC grid connection can be more efficient while the required conversion stages are decreased [3].

PV modules can be connected to the grid with central, string or module integrated converters [4]. In string and central converters, serial and parallel connections of PV modules are utilized. Hence, they do not serve good performance under mismatch losses of PV modules and non-uniform irradiation conditions [5]. Since module integrated converters can harvest maximum energy of each module, they can be more efficient [6].

Module integrated converters are generally designed as isolated. Isolated converters consist of high frequency operated transformer, in return they can have high step-up ratio [7]. In literature, Boost Full-Bridge Isolated Converters (BFBIC) [8] and resonant behavior-based converters [9] are popular. However, BFBIC has some issues such as hard switching, high number of semiconductors because of two-stage conversion, and large magnetic core size for input inductance. Moreover, resonant converters have complex control methods which need adjusting switching frequency accurately and have high peak and RMS currents because of the resonance behavior.

Dual Active Bridge (DAB) converter [10], serves soft switching by using the leakage inductance's energy and switches are exposed only input or output voltage levels. Numerous modulation methods [10]–[13] are proposed for modulating the current of DAB converters. Among them, Discontinuous Conduction Mode (DCM) based, hybrid current modulation (HCM) [11] can bring the advantages of smaller magnetic components, low EMI, easy control, and high step-up ratio.

In [14], HCM DAB PV DC/DC converter is proposed. However, in this study, Partial Shading (PS) was taken into consideration which can happen especially for rooftop PV modules. In this design, the converter was designed under the consideration of wide input voltage range. Hence, it can have higher RMS/peak currents and magnetic core size. On the other hand, PS rarely occurs for the PV modules in PV farms, and annual energy loss from PS is reported between 3%-6% [15]. Therefore, designing a PV converter considering uniform irradiation (UI) conditions can be more effective for PV farms.

In this study, the design method of HCM DAB PV DC/DC converter is given for UI conditions, and its performance evaluated versus the design of PS case.

The rest of the paper is organized as follows. In the next section, PV module's characteristic is presented. The operation modes and design strategy of HCM DAB DC/DC converter are given Section 3. Comparison of designs for UI and PS cases are served in Section 4. Finally, section 5 concludes the paper.

2. Analysis of PV Module's Characteristic under Uniform Irradiation Conditions

PV cells are connected serially to produce PV modules, and they can be modelled with single-diode electrical equivalent PV cell model which is given in Fig. 1. The voltage-current relationship of a cell [16] can be written as,

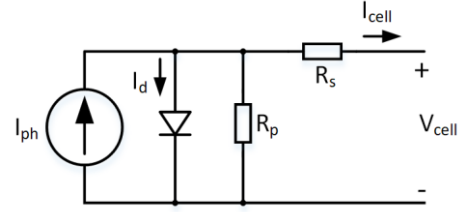


Figure 1. Single-diode electrical equivalent model for a PV cell.

Table 1. CS6P-250M PV Module Parameters under the test conditions of 1000 W/m², 25°C, and air mass 1.5.

Parameters	Values
Maximum output power, P_m [W]	250
Open circuit voltage, V_{oc} [V]	37.5
Short circuit current, I_{sc} [A]	8.74
Voltage at maximum power, V_m [V]	30.4
Current at maximum power, I_m [A]	8.22
Number of series connected cells, N_s	60
Temperature coef. for I_{sc} , α_i	0.06 %/°C
Photocurrent, I_{ph} [A]	8.74
Saturation current of the diode, I_s [A]	2.353×10^{-10}
Modif. diode ideality factor, α	1.54
Total series resistance, R_s [Ω]	0.282
Total parallel resistance, R_p [Ω]	257.75

$$I_{cell} = I_{ph} - I_s \left(e^{\frac{V_{cell} + I_{cell} R_s}{a}} - 1 \right) - \frac{V_{cell} + I_{cell} R_s}{R_p} \quad (1)$$

Where I_{ph} and I_s are photocurrent and diode saturation current, respectively. In addition, the cell parameters are given as follows: V_{cell} is the cell voltage, I_{cell} is cell current, R_s is the series resistance, R_p is the parallel resistance. Moreover, a is the modified diode ideality factor which can be calculated by $a = AkT_c N_s / q$. A is the diode ideality factor, k Boltzmann constant (1.380649×10^{-23} J·K⁻¹), q is the electron charge ($1.602176634 \times 10^{-19}$ C), T_c is the temperature of cell in Kelvin and N_s is the number of serially connected cells.

The I_{ph} and I_s are dependent on operating temperature of the cell T_c and cell temperature under Standard Test Conditions (STC) $T_{c,STC}$ [16].

$$I_{ph} = \frac{G}{G_{STC}} (I_{sc,STC} + \alpha_i (T_c - T_{c,STC})) \quad (2)$$

$$I_s = I_{s,STC} \left(\frac{T_c}{T_{c,STC}} \right)^3 e^{\left(\frac{1}{k} \left(\frac{E_{g,STC}}{T_{c,STC}} - \frac{E_g}{T_c} \right) \right)} \quad (3)$$

where G is irradiance (W/m²) on the PV module, α_i is the short circuit current's temperature coefficient. $I_{sc,STC}$ and $I_{s,STC}$ are the short circuit current and the saturation current of the diode under STC, respectively. E_g is the band gap energy, and $E_{g,STC}$ is the band gap energy under STC (1.6 eV). On the other hand, E_g also depends on the temperature, and its relationship is given below [17].

$$E_g = E_{g,STC} (1 - 0.0002677 (T_c - T_{c,STC})) \quad (4)$$

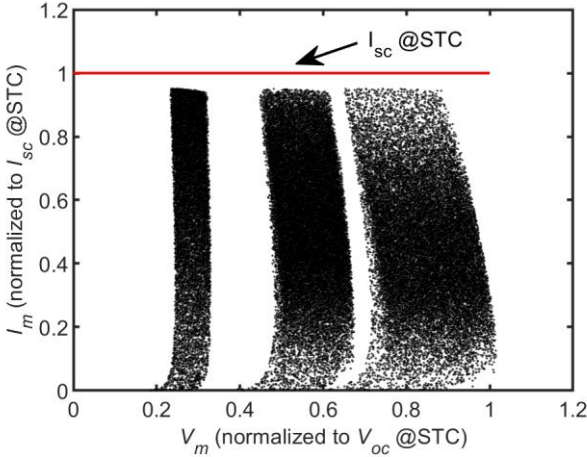


Figure 2. MPP voltage-current points under random irradiation conditions for three groups (Partial shading case) [14].

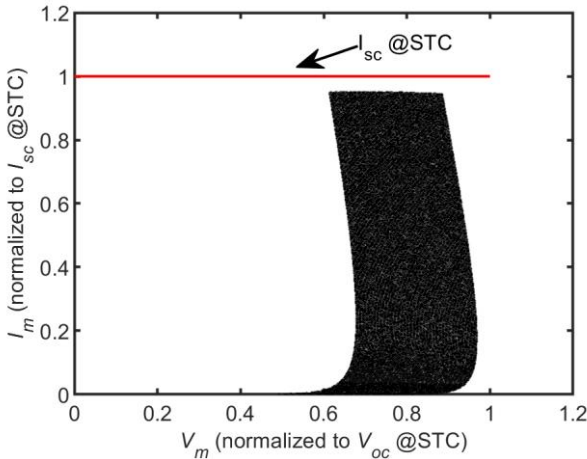


Figure 3. MPP voltage-current points under uniform irradiation conditions.

The temperature of the cell can be predicted by using the ambient temperature T_a , and Nominal Operating Cell Temperature NOCT, which is given in producer's datasheets, such as [18],

$$T_c = T_a + (NOCT - 20) \frac{G}{800} \quad (5)$$

In this study, parameters of CS6P-250M PV module, which are listed in Table 1, are used in analyses and simulations. This PV module has serially connected 60 cells. These cells are grouped in three group (seen in Fig. 4), and each group has an anti-parallel diode to prevent PV module from hot spots under partial shading. In [14], random irradiation levels for each group are used for calculating maximum voltage-current points, and result is given in Fig. 2. In this case, partial shading occurs and Maximum Power Point (MPP) voltage scatters in a wide range such as between 0.22 times to 1.02 times of open circuit voltage at STC $V_{oc,STC}$. However, in a PV farm this situation rarely occurs [15]. Hence, using uniform irradiation in analysis for each group can be more accurate for PV farm cases. When 10^5 random irradiation

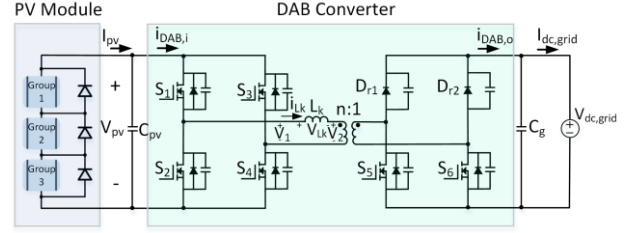


Figure 4. HCM DAB PV DC/DC converter.

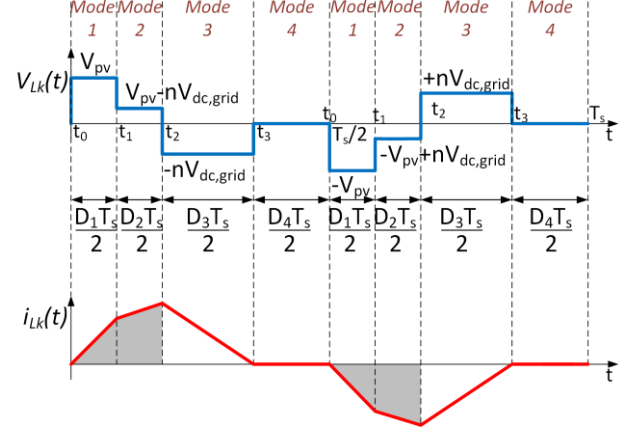


Figure 5. Illustration of four distinct operation Modes. values from 0 W/m² to 1000 W/m² and random ambient temperature values from -25 °C to +50 °C are used, the MPP current-voltage points are obtained as given in Fig.3. The minimum MPP voltage is 20V and maximum MPP voltage is 38.25 V is obtained. On the other hand, maximum MPP current is always smaller than $I_{sc,STC}$. Hence, in this paper these criteria are used.

3. HCM DAB PV DC/DC Converter

PV module integration to DC grid with hybrid current modulated DAB DC/DC converter is shown in Fig. 4. Hybrid current modulation uses triangular (TRM) and trapezoidal (TzM) current modulations in proper voltage regions to decrease the RMS current of the transformer's primary side.

The TRM is a version of TzM, and it doesn't have Mode 3. The four distinct operation modes for the positive half of switching cycle are described below, and for the negative switching cycle turned-on/off switches are given in brackets. Moreover, important voltage-current waveforms of modes are shown in Fig.5, and current-voltage values during these modes are summarized below:

Mode 1 [$t_0 < t < t_1$]: Because of the DCM operation, the leakage inductance's current is zero at t_0 . When the switches of S_1, S_4 and S_5 (S_2, S_3 and S_6) are turned on, the current of leakage inductance increases as follows,

$$i_{Lk}(t) = \frac{V_{pv}}{L_k} t \quad (6)$$

where V_{pv} is the PV module's MPP voltage and L_k is the leakage inductance's value.

Mode 2 [$t_1 < t < t_2$]: In this mode, energy is taken from PV and delivered to DC grid at the same time. At time t_1 , the S_5 (S_6) is turned off and D_{r1} (D_{r2}) starts freewheeling the

current. The current equation can be written as:

$$i_{Lk}(t) = i_{Lk}(t_1) + \frac{V_{pv} - nV_{dc,grid}}{L_k}(t - t_1) \quad (7)$$

Where $V_{dc,grid}$ is the voltage of DC grid and n is the transformer's turn ratio. As can be interpreted from (7), the current can increase or decrease during this mode which depends on the input and reflected output voltage values. If the current slope is negative, and when it reaches zero Mode 3 will not exist.

Mode 3 [$t_2 < t < t_3$]: At the instant t_2 the S_1 (S_2) is turned off and S_2 's diode D_2 (S_1 's diode D_1) starts conducting the current. Hence, the current of the leakage inductance decreases during this mode as follows,

$$i_{Lk}(t) = i_{Lk}(t_2) + \frac{-nV_{dc,grid}}{L_k}(t - t_2) \quad (8)$$

Mode 4 [$t_3 < t < T_s/2$]: At the end of Mode 3 (at the instant t_3), the leakage inductance's current falls to zero, and stays at zero during Mode 4.

When the current taken from PV module is calculated by using the average currents of Mode 1 and Mode 2, (9) can be obtained.

$$I_{pv} = \frac{D_h^2}{4L_k f_s} (V_{pv} - m_i^2 n V_{dc,grid}) \quad (9)$$

In this equation, D_h is the duty cycle of hybrid current modulation and m_i is the modulation index. These parameters are defined as follows,

$$D_h = D_1 + D_2 \quad (10)$$

$$m_i = \frac{D_2}{D_h} \quad (11)$$

Where D_1 and D_2 are the duty ratios of Mode 1 and Mode 2, respectively. To guarantee DCM operation, maximum duty cycle value can be calculated by the help of $D_1 + D_2 + D_3 \leq 1$. In addition, D_3 (duty of Mode 3) can be expressed by using (6), (7), and (8) as follows,

$$D_3 = D_h(\lambda - m_i) \quad (12)$$

By using (10), (11) and (12), maximum duty ratio can be found as,

$$D_h \leq 1/(1 - m_i + \lambda) \quad (13)$$

In addition, D_h must be ≤ 1 , so m_i must be $\leq \lambda$ (from (13)). In addition, when m_i equals to λ , Mode 3 will not exist and TRM operation will be obtained.

The converter can operate with different m_i and D_h pairs. These parameters also determine the required leakage inductance value. Operating with maximum duty value D_h , minimizes the RMS currents [14]. Since conduction losses and switching losses (due to increase of peak currents) depends on RMS currents, minimizing the RMS currents will decrease the total loss. Hence, in this paper, RMS current minimization way is exploited for determining the proper parameters of n , L_k and m_i .

(13) and maximum PV current $I_{sc,stc}$ is used in (9), the calculated m_i value can be written as follows,

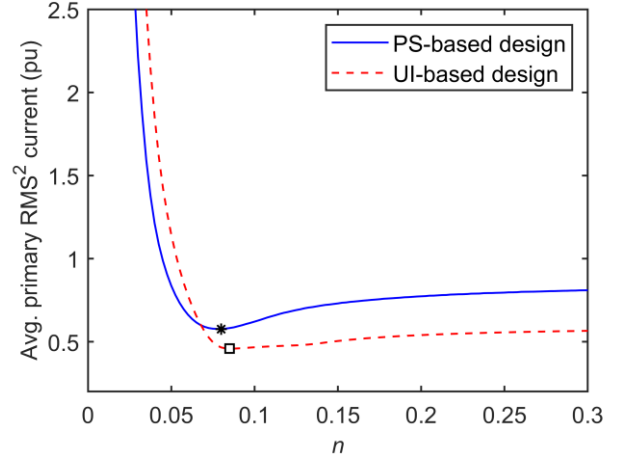


Figure 6. Avg. RMS² currents versus n (normalized to $I_{sc,stc}^2$).

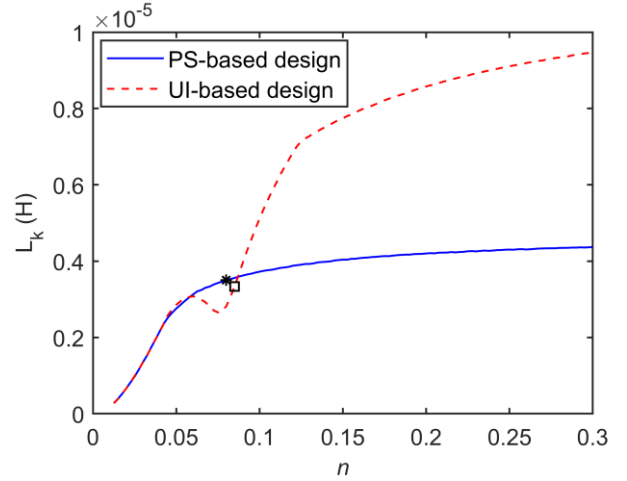


Figure 7. Optimum L_k values for PS-based and UI-based designs.

$$m_{i,calc} = \sqrt{\frac{x^2(y-z) - zy(x+y)}{x(x+z)^2}} + \frac{z(x+y)}{x(z+x)} \quad (14)$$

Where x , y and z are defined as,

$$x = nV_{dc,grid} \quad (15)$$

$$y = V_{pv} \quad (16)$$

$$z = 4I_{sc,stc}L_k f_s \quad (17)$$

The optimum m_i value equals to $m_{i,calc}$, and its maximum limits are $m_{i,calc} \leq \lambda$ and $m_{i,calc} < 1$ from (13) and (11).

4. Comparison of UI and PS-Based Designs of HCM DAB PV DC/DC Converter

The Genetic Algorithm (GA) is used to find optimum operation point (the pair of n and L_k) which gives minimum average RMS² current. For this reason (6)-(17), and the MPP data which are given in Fig. 2 and Fig. 3 are used. The average RMS² current affects conduction losses and its (18) chosen as the cost function as follows,

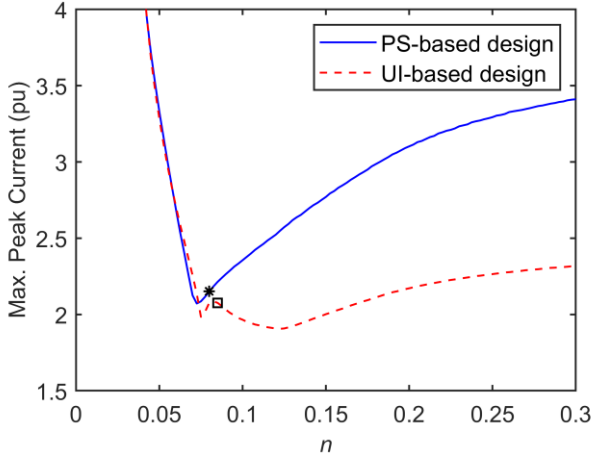


Figure 8. Max. peak currents versus n (normalized to $I_{sc,stc}$).

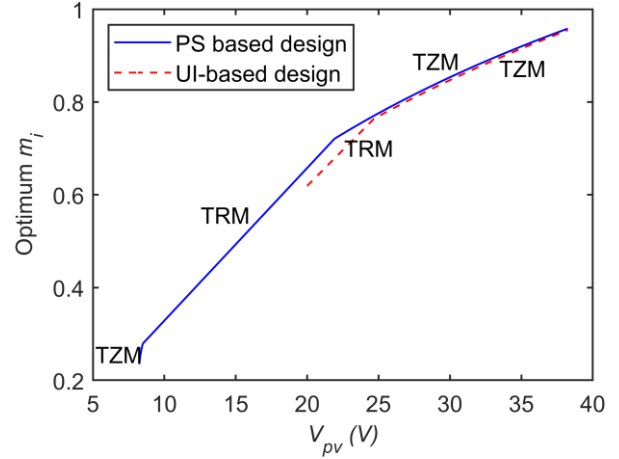


Figure 10. Optimum m_i values versus V_{pv} .

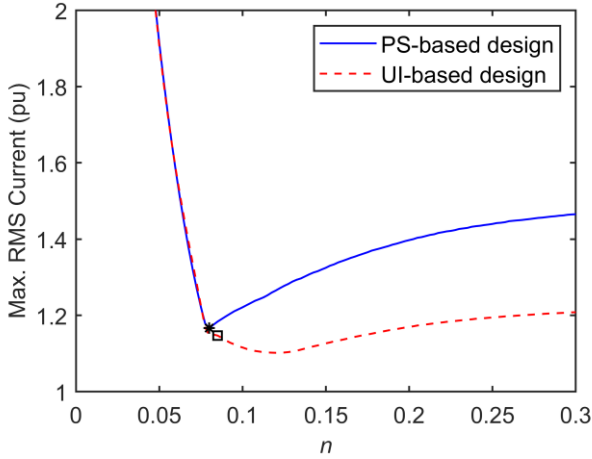


Figure 9. Max. RMS currents versus n (normalized to $I_{sc,stc}$).

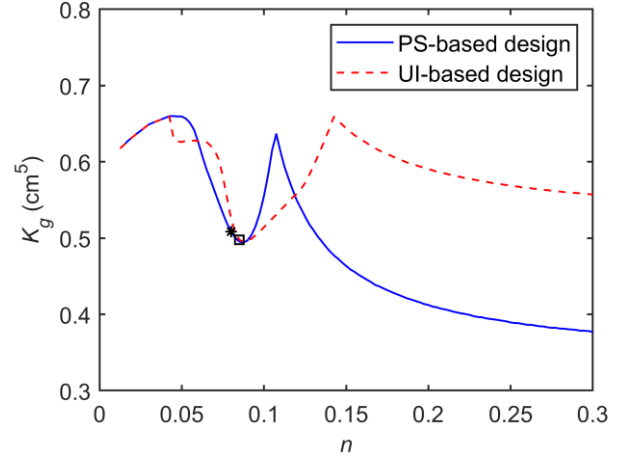


Figure 11. Minimum required transformer size versus n .

$$I_{RMS,avg}^2 = \frac{1}{10^5} \sum_{k=1}^{10^5} I_{RMS}^2(k) \quad (18)$$

Where k is the number of random temperature-irradiation pairs. By using 10^5 irradiation and temperature values, the (18) is minimized by GA and the results are given in Fig. 6. Minimum RMS² values of both operation is marked on with star (for PS) and square (for UI) in this figure. Optimum n values are 0.08 and 0.085 for PS and UI-based designs, respectively. These n values are used for further comparisons.

In Fig. 7, optimum L_k values versus n are given. At optimum n values, 3.5 μ H and 3.33 μ H inductance values are found for PS and UI-based designs, respectively.

Since designers chose semiconductor switches with the knowledge of maximum RMS and peak currents, Fig. 8 and Fig. 9 are drawn. At optimum n values, UI-based design has 3.56% smaller maximum peak current and 3.88% smaller RMS² current than PS-based design.

The optimum m_i value versus PV voltage graph is given for PS and UI-based designs in Fig. 10. Since, PS-based design operates also at small input voltages, the graph

Table 2. Five different operation scenarios for the comparison.

Case Number	Irradiation [W/m ²]	Cell Temp. [°C]	V_{mpp} [V]	I_{mpp} [A]
1	1000, UI	6.25	33.15	8.25
2	1000, UI	25	30.4	8.22
3	800, UI	45	28	6.66
4	916, UI	66.62	25	7.62
5	1000, 1000, 0	25	20.26	8.22

was drawn from 8.25 V. On the other hand, UI-based design utilizes slightly smaller m_i values than PS-based design.

The magnetic core size can be another important parameter for comparison. An approach to define the minimum core size of the transformer is given in [19] as follows,

$$K_{g,tf} \geq \frac{\rho(nV_{dc,grid}t_{ap}/2)^2 I_{tot}^2}{\Delta B^2 K_u P_{cu}} 10^8 (cm^5) \quad (19)$$

In this equation, ΔB is the peak value of the flux density,

Table 3. Peak and RMS current of PS and UI-based designs for four different irradiation and cell temperature cases.

Case Number	I_{peak} [A]		I_{RMS} [A]	
	PS	UI	PS	UI
1	13.71	11.20	9.98	9.37
2	10.40	11.91	9.36	9.10
3	11.24	12.71	7.80	7.80
4	14.32	16.31	8.73	9.08
5	17.85	19.27	9.90	10.25

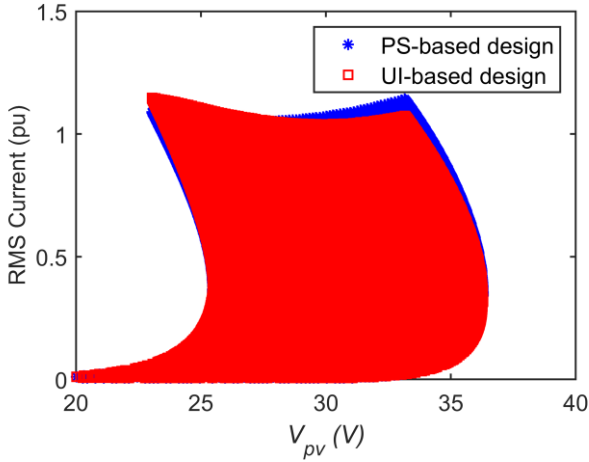


Figure 12. RMS currents versus PV voltage for 10^5 random irradiations-temperatures of UI (current normalized to $I_{sc,STC}$).

t_{ap} is the time duration of applied voltage to the transformer's winding, I_{tot} is total RMS current of windings which is reflected to the primary winding, and P_{cu} is the total copper loss. If (19) is calculated with the values of $\rho=1.72 \times 10^{-6} \Omega\text{cm}$, $P_{cu}=4 \text{ W}$, $\Delta B=35 \text{ mT}$ and $K_u=0.5$, the Fig. 11 is obtained. Minimum core sizes are calculated as 0.51 cm^3 and 0.498 cm^3 for PS-based and UI-based designs, respectively. Hence UI-based design can utilize a smaller core size.

In order to validate analysis, PSIM® simulations were performed. For this aim, five irradiation-temperature cases were chosen, and they are listed in Table 2. The first four of them are for UI, and the last one is for PS. Under these cases, measured peak currents and primary RMS currents were tabulated in Table 3. It can be seen from this table that UI-based design has smaller RMS currents than PS-based design at higher voltages ($\geq 28 \text{ V}$). In addition, this result can also be proven with the calculations which are given in Fig. 12 for 10^5 data (data which are used for UI conditions).

On the other hand, RMS current of the UI-based design can be interpreted high when only Table 3 is thought. However, in this table, maximum peak current case of PS-based design (18.81 A) is not given, which occurs at 16.46 V. In this voltage level, UI-based design doesn't work.

For case number 2, which is STC's case, current shapes of leakage inductances are taken from PSIM, and they are

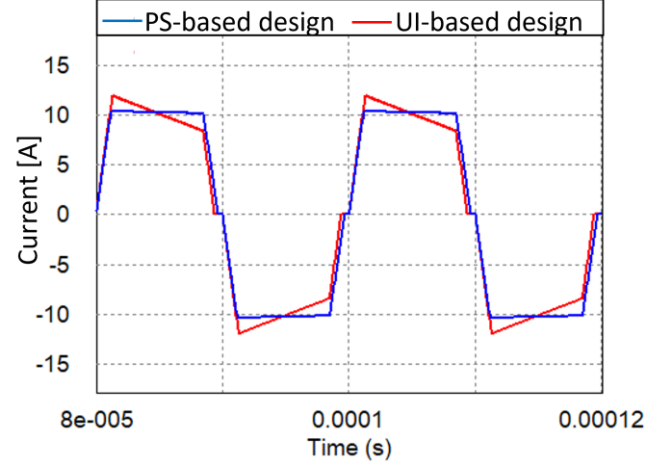


Figure 13. Current shapes of leakage inductances for PS and UI-based design under STC's irradiation and cell temperature ($f_s=50 \text{ kHz}$, $V_{dc,grid}=380 \text{ V}$).

given in Fig. 13. Although peak current of UI-based design is higher, the RMS² current of UI-based design is 5.47% smaller than PS-based design (as seen in Table 3) for STC.

5. Conclusions

In this paper, HCM DAB PV DC/DC converter is analyzed, and a design method was presented for uniform irradiation conditions. Analyses show that UI-based design methodology utilizes smaller leakage inductance value and higher turn ratio. With the help of this, it can decrease the maximum value of primary RMS² current by 3.88%, maximum peak current by 3.56%, and minimum required core size by 2.35%. When the module integrated converters are used in PV farms, where partial shading rarely occurs, UI-based design of HCM DAB PV DC/DC converter can be more suitable than partial shading design. In addition, RMS² current advantage of the UI-based design becomes more effective when PV module operates vicinity of STC's MPP voltage and at higher input voltage values ($\geq 28 \text{ V}$).

On the other hand, since UI-based design utilizes minimum MPP voltage value as 20 V, it can also operate under slightly partial shading conditions.

6. References

- [1] IEA, "Renewables 2022," *Reporte*, 2022.
- [2] Kouro, S., Leon, J. I., Vinnikov, D., and Franquelo, L. G., "Grid-connected photovoltaic systems: An overview of recent research and emerging PV converter technology," *IEEE Industrial Electronics Magazine*, vol. 9, no. 1, 2015.
- [3] Wang, P., Goel, L., Liu, X., and Choo, F. H., "Harmonizing AC and DC: A Hybrid AC/DC future grid solution," *IEEE Power and Energy Magazine*, vol. 11, no. 3, 2013.
- [4] Yuan, X., and Zhang, Y., "Status and opportunities of photovoltaic inverters in grid-tied and micro-grid systems," in *Conference Proceedings - IPEMC 2006: CES/IEEE 5th International Power Electronics and Motion Control Conference*, 2007.
- [5] Walker, G. R., and Pierce, J. C., "Photovoltaic DC-DC module integrated converter for novel cascaded and

- bypass grid connection topologies -Design and optimisation," in *PESC Record - IEEE Annual Power Electronics Specialists Conference*, 2006.
- [6] Edwin, F., Xiao, W., and Khadkikar, V., "Topology review of single phase grid-connected module integrated converters for PV applications," in *IECON Proceedings*, 2012.
- [7] Forouzesh, M., Siwakoti, Y. P., Gorji, S. A., Blaabjerg, F., and Lehman, B., "Step-Up DC-DC converters: A comprehensive review of voltage-boosting techniques, topologies, and applications," *IEEE Trans Power Electron*, vol. 32, no. 12, 2017.
- [8] Guo, K., Cui, L., Mao, M., Zhou, L., and Zhang, Q., "An Improved Gray Wolf Optimizer MPPT Algorithm for PV System with BFBIC Converter under Partial Shading," *IEEE Access*, vol. 8, 2020.
- [9] Zhao, X., Chen, C. W., and Lai, J. S., "A High-Efficiency Active-Boost-Rectifier-Based Converter with a Novel Double-Pulse Duty Cycle Modulation for PV to DC Microgrid Applications," *IEEE Trans Power Electron*, vol. 34, no. 8, 2019.
- [10] De Doncker, R. W. A. A., Divan, D. M., and Kheraluwala, M. H., "A Three-Phase Soft-Switched High-Power-Density DC/DC Converter for High-Power Applications," *IEEE Trans Ind Appl*, vol. 27, no. 1, 1991.
- [11] Zengin, S., and Boztepe, M., "A Novel Current Modulation Method to Eliminate Low-Frequency Harmonics in Single-Stage Dual Active Bridge AC-DC Converter," *IEEE Transactions on Industrial Electronics*, vol. 67, no. 2, 2020.
- [12] Krismer, F., and Kolar, J. W., "Closed form solution for minimum conduction loss modulation of DAB converters," *IEEE Trans Power Electron*, vol. 27, no. 1, 2012.
- [13] Bai, H., and Mi, C., "Eliminate reactive power and increase system efficiency of isolated bidirectional dual-active-bridge dc-dc converters using novel dual-phase-shift control," *IEEE Trans Power Electron*, vol. 23, no. 6, 2008.
- [14] Zengin, S., "A hybrid current modulated DAB DC/DC converter for connecting PV modules to DC grid considering partial shading," *Computers and Electrical Engineering*, vol. 101, 2022.
- [15] García, M., Vera, J. A., Marroyo, L., Lorenzo, E., and Pérez, M., "Solar-tracking PV plants in Navarra: A 10 MW assessment," *Progress in Photovoltaics: Research and Applications*, vol. 17, no. 5, 2009.
- [16] Petrone, G., Ramos-Paja, C. A., and Spagnuolo, G., *Photovoltaic Sources Modeling*. 2017.
- [17] De Soto, W., Klein, S. A., and Beckman, W. A., "Improvement and validation of a model for photovoltaic array performance," *Solar Energy*, vol. 80, no. 1, 2006.
- [18] Sun, V., Asanakham, A., Deethayat, T., and Kiatsiriroat, T., "A new method for evaluating nominal operating cell temperature (NOCT) of unglazed photovoltaic thermal module," *Energy Reports*, vol. 6, 2020.
- [19] Erickson, R. W., and Maksimovic, D., *Fundamentals of Power Electronics*, 2001.